Measurement report: Aircraft observations of aerosol and microphysical quantities of stratocumulus in autumn over Guangxi Province, China: daylight variation, vertical distribution and aerosol-cloud interactions

Sihan Liu[a], Honglei Wang[a*], Delong Zhao[b c*], Wei Zhou[d], Yuanmou Du[d], Zhengguo Zhang[e], Peng Cheng[e], Tianliang Zhao[a], Yue Ke[a], Zihao Wu[a], Mengyu Huang[d]

[a] China Meteorological Administration Aerosol-Cloud and Precipitation Key Laboratory, Nanjing University of Information Science and Technology, Nanjing 210044, China

[b] Weather Modification Centre, China Meteorological Administration (CMA), Beijing 100081, China

[c] Field experiment base of cloud and precipitation research in North China, China Meteorological Administration, Beijing 101200, China.

[d] Beijing Weather Modification Center, Beijing 100089, China

[e] Weather Modification Office of Guangxi Zhuang Autonomous Region, Nanning 530022, China

*Corresponding author.

E-mail address: hongleiwang@nuist.edu.cn (H. Wang) and zhaodelong@bj.cma.gov.cn(D. Zhao)

Abstract: Aerosols and clouds play essential roles in the global climate system, and aerosol-cloud interactions have a significant impact on the radiation balance, water cycle, and energy cycle of the earth-atmosphere system. To understand the effect of aerosols on the vertical distribution of stratocumulus microphysical quantities in southwest China, we analyzed data from nine aircraft observations over Guangxi from October 10 to November 3, 2020. This analysis focused on the daylight variation characteristics and formation mechanisms of stratocumulus microphysical profiles, considering the influence of aerosol number concentration in relation to the source of air mass and individual cases. Aerosol number concentration (Na) and cloud droplet concentration (Nc) decreased gradually with the altitude increase below 1500m and did not change with the height between 1500 m and 3300 m. The temperature inversion layer at the top of the planetary boundary layer (PBL) hindered the increase in the cloud droplet particle size. The lower layer of the

stratocumulus cloud in Guangxi mainly contained small-sized cloud droplets (effective diameter of

a cloud droplet, $E_d<15$ μm), and the middle and upper layers of cloud droplets were large particle-

size cloud droplets ($E_d>20$ μm). The vertical distribution of cloud microphysical quantity had

apparent daylight variation. When aerosols in PBL were transported to the upper air (14:00 to 20:00),

Nc in the lower layer decreased, and the small particle-size cloud droplets ($E_d <20$ μm) in the middle

layer and upper layer increased. Aerosols from the free atmosphere were transported into PBL

(10:00 to 13:00), providing an abundance of cloud condensation nuclei, which increased the number

of small particle-size cloud droplets in the lower layer of the cloud (near the top of PBL). The

characteristics of cloud microphysical quantities (Nc and E_d) were also affected by the source of air

mass and the height of PBL. Na and Nc were high under the influence of land air mass or aerosols

within PBL, and the cloud droplet number concentration spectrum was unimodal. Na and Nc were

low under the influence of marine air mass or above the boundary layer, and the cloud droplet

number concentration spectrum was bimodal. The relationship between stratocumulus and aerosol

in this region is consistent with the Twomey effect. E_d and Na remain negatively correlated in

different liquid water content ranges, and FIE (the aerosol first indirect effect) ranged from -0.07 to

-0.58.

Keywords: Aerosol; Aircraft observations; Cloud microphysical quantities; Vertical profile; The

planetary boundary layer

1. Introduction

Clouds are an essential component of the Earth-atmosphere system, covering over 67% of the

Earth's surface (King et al., 2013), with stratocumulus clouds covering approximately 20% of the

Earth's surface in the annual mean. Stratocumulus typically occupies the upper few hundred meters

of the planetary boundary layer (PBL) (Wood, 2012). They can absorb atmospheric long-wave

radiation and reflect solar short-wave radiation to influence the radiation budget of the Earth's

atmospheric system (Pyrina et al., 2015; Ramanathan et al., 1989; Zelinka et al., 2014). Additionally,

they participate in the global water cycle through precipitation processes (Betts, 2007; Rosenfeld et

al., 2014). Cloud microphysical characteristics are closely related to the climate effect and

precipitation formation of stratocumulus clouds. Differences in cloud water content, cloud droplet

number concentration and cloud droplet size in different regions will produce different radiative

forcing and precipitation (de Boer et al., 2008; Waliser et al., 2011; Yuan et al., 2008).

59   Aerosols are an important source of cloud condensation nuclei (CCN), and thus, variations in

60   aerosols can lead to significant changes in the microscopic characteristics of clouds (Chen et al.,

61   2021; Dusek et al., 2006; Lance et al., 2004). Twomey (1977) suggested that, with the liquid water

62   path (LWP) of clouds remaining constant, an increase in aerosol number concentration (Na) would

63   lead to an increase in cloud droplet number concentration (Nc) and a decrease in cloud droplet size,

64   thereby enhancing cloud albedo. Albrecht (1989) proposed that the decrease of cloud droplet particle

65   size caused by the increase of aerosols would further inhibit the precipitation process of clouds and

66   thus extend the lifetime of clouds.

67   Currently, aircraft observation, ground-based remote sensing, and satellite remote sensing are

68   the main observation methods used to study the interaction between aerosols and clouds. Many

69   scholars have confirmed the Twomey effect (the first indirect effect of aerosols) through

70   observational data (Ferek et al., 1998; Han et al., 1994; Kleinman et al., 2012; Koren et al., 2005).

71   Based on radar observation data, Kim et al. (2003) found that the aerosol optical depth in Oklahoma

72   presents a linear proportional relationship with LWP on a completely cloudy day with a single-layer

73   cloud, and the effective radius of cloud droplets is negatively correlated with the surface aerosol

74   light scattering coefficient. For a given LWP, Cloud albedo and radiative forcing are very sensitive

75   to the effective radius. Li et al. (2019) using aircraft observation data over the Loess Plateau, found

76   a negative correlation between Na and Nc in both vertical and horizontal directions. Under high

77   aerosol loading (Na below the cloud base was 4573 cm^{-3}), smaller cloud droplets with high Nc

78   (Nc=157 cm^{-3}) were observed, while few large cloud droplets (Nc=118 cm^{-3}) were formed under

79   low aerosol loading (Na below the cloud base was 982 cm^{-3}). Cloud droplet number concentration

80   was negatively correlated with cloud droplet diameter within a specific range of liquid water content

81   (LWC). However, some scholars have also observed a positive correlation between Na and the

82   effective diameter of cloud droplets (E_d) (Harikishan et al., 2016; Jose et al., 2020; Liu et al., 2020),

83   referred to as the anti-Twomey effect.

84   Aircraft observations with continuous vertical sampling are the most reliable source that can

85   accurately characterize the vertical relationship between aerosol and cloud (Nakajima et al., 2005;

86   Terai et al., 2014; Wehbe et al., 2021; Zaveri et al., 2022). McFarquhar et al.(2021) conducted

87   aircraft observations in the Southern Ocean region. They found aerosols above clouds may originate

88   from new particle formation and remote transport from continental air masses. This leads to

89   variations in CCN and Nc near cloud tops. During the ACE-ENA campaign, the probability of

90   aerosol transport interacting with marine boundary layer clouds over the eastern North Atlantic

91   (ENA) during summer was approximately 62.5% (Wang et al., 2020).

92   Zhao et al.(2019) observed a stratus cloud (water cloud) in the Huanghua region of China by

93   aircraft and found that in the PBL, the effective radius of cloud droplets and Na show a negative

94   relationship, while they showed a clear positive relationship in the upper layer above PBL with

95   much less Na. It also shows that the relationship between the effective radius of cloud droplets and

96   Na changes from negative to positive when LWC increases. Lu et al. (2007) compared the

97   microphysical quantities of stratocumulus clouds influenced by aircraft flight tracks and those in

98   undisturbed regions and found that the effective radius of cloud droplets in the flight path region

99   was smaller, the number concentration of cloud drops was lower, and the cloud LWC was larger,

100   providing observational evidence for the first indirect effect of aerosols.

101   The mechanism of interaction between aerosols and clouds still involves significant uncertainty,

102   influenced by factors such as aerosol physicochemical properties, meteorological conditions, cloud

103   types, and the relative positioning of aerosols and cloud layers (Almeida et al., 2014; Dusek et al.,

104   2006; Wex et al., 2010; Zhang et al., 2011). Therefore, precise measurements of cloud microphysical

105   properties are crucial as the first step in studying aerosol-cloud interactions. Multi-aircraft

106   observations provide high-precision observational data, aiding in understanding the relationship

107   between aerosols and cloud microphysical characteristics.

108   Our study on the vertical distribution of aerosol in the Guangxi region found that the vertical

109   profile of Na in this region has prominent daylight variation characteristics under the influence of

110   PBL. In the morning, aerosols are mainly concentrated in PBL. With the development of PBL and

111   the enhancement of turbulent activity, the aerosols near the ground are diluted in the afternoon, and

112   aerosols can be transmitted to more than 2 km. At night, the rapid decline of the top of PBL will

113   increase Na near the surface. At the same time, some aerosols will stay above the top of PBL,

114   forming a high-concentration aerosol layer (Liu et al., 2024). Previous studies have shown that

115   aerosols can affect cloud microphysical properties. When aerosol particles settle onto clouds or the

116   cloud top is elevated, aerosols can alter the microphysical characteristics of clouds by being

117   entrained into the cloud top (Lu et al., 2018; Painemal et al., 2014). This study used data from nine

118   cloud-penetrating aircraft flights to investigate the vertical distribution and formation mechanisms

of cloud microphysical properties in stratocumulus clouds over Guangxi. Additionally, we discussed the differences in the impact of aerosols from different sources on cloud microphysical properties. Our findings indicate that the interaction between aerosols and clouds in this region aligns with the Twomey effect. The ultimate goal is to provide observational constraints for the simulation of aerosol radiative forcing in global climate models.

2. Data and methodology

2.1. Aircraft data and reanalyze data and data processing

The Beijing Weather Modification Office (BJWMO) provided the data for this study, and nine flights of stratocumulus clouds and aerosols over Guangxi were conducted using the King Air 350 ER turbo aircraft. The aircraft is equipped with the Aircraft Integrated Meteorological Measurement System (AIMMS-20, Aven tech Inc., Canada), which provides meteorological elements such as temperature (T) and relative humidity (RH) with a time resolution of 1 s. A passive cavity aerosol spectrometer probe (PCASP-100X, DMT Inc, USA) was installed to provide aerosol number concentrations in the optical particle size range of 0.11 to 3 μm, with a time resolution of 1s, particle size uncertainty of 20%, and concentration uncertainty of 16%. The Fast Cloud Droplet Probe (FCDP, SPEC Inc, USA) was used to observe the cloud droplet concentration, cloud particle concentration and cloud particle size distribution. Its principle is to detect particles with an optical diameter ranging from 2 μm to 50 μm using forward scattering technology with a time resolution of 1s. The particle number concentration measured by the FCDP in the size range of less than 3 μm has significant uncertainty. In this study, the range of Nc is defined as 3-50 μm. Na and Nc are measured in volume units. All instruments were calibrated before observation. The detailed principles of the airborne instruments can be found in the following studies (Collaud Coen et al., 2010; Strapp et al., 1992; Zhang et al., 2009).

Table 1 Flight information for the measurement campaign (Na, Nc, LWC, and Ed values are averages ± the standard deviations).

Date	Take-off/landing time (Beijing time)	Cloud base/cloud top height (m)	Inside cloud Na (cm^{-3})	Nc (cm^{-3})	LWC (g·m^{-3})	E$_d$ (μm)
20201010	11:53–15:50	1203-1652	355±157	586±328	0.45±0.30	12.25±1.92
20201011	14:26–17:53	1261-1542	636±290	529±350	0.19±0.14	9.45±1.30

20201025	09:34–12:58	1076-3298	9±31	38±35	0.18±0.15	26.96±9.80
20201026	09:53–13:29	1367-3146	5±19	35±27	0.10±0.09	21.86±8.77
20201028	14:05–17:27	1664-2729	239±229	354±502	0.45±0.43	16.90±9.54
20201029	10:05–13:33	516-3266	1402±569	396±289	0.17±0.16	9.86±2.54
20201101	18:17–22:06	1661-2715	333±170	199±80	0.35±0.17	17.93±4.71
20201102	14:04–17:41	696-3145	177±174	136±97	0.22±0.15	17.45±3.51
20201103	14:17–17:28	2021-2938	44±30	139±57	0.29±0.10	15.73±3.56

144 Detailed data of this aircraft observation activity, including observation date, time, cloud

145 thickness and microphysical quantities, are summarized in Table 1. Compared with aircraft

146 observation data in other regions, the average LWC in Guangxi was higher, 5.33 times that in North

147 China, and the average cloud droplet diameter was larger, 2.58 times that in North China (Zhao et

148 al., 2011). Compared with the Marine Stratocumulus (Lu et al., 2011; Miles et al., 2000), the

149 Stratocumulus in Guangxi had higher cloud base height and greater cloud thickness. The cloud

150 microphysical characteristics of the stratocumulus observed in this study are similar to those of

151 previous observations. Compared with stratocumulus (non-precipitation warm cloud) over eastern

152 China, the Nc, LWC and E_d of stratocumulus in Guangxi region were larger. According to previous

153 studies (Liu et al., 2024), there were no special weather processes in the upper air and on the ground

154 in Guangxi during the observation period, which ensured the quality of the data and the universality

155 of the conclusions.

156 To ensure data quality, this study selected the data that met the following conditions and the

157 flight macro record as the in-cloud data: Nc ≥ 10 cm^{-3}, LWC ≥ 10^{-3} g·m^{-3} (Gunthe et al., 2009; Zhang

158 et al., 2011). The observation records show that the clouds during the observation period were

159 stratocumulus clouds (non-precipitation warm clouds). Therefore, the aerosol and cloud

160 microphysical data met the following conditions: observation height ≤ 4000 m, T > 0 ℃. The height

161 of PBL is determined by applying the gradient method to the vertical distribution of potential

162 temperature (Kim et al., 2007; Su et al., 2017).

163 The microphysical quantities such as Nc, LWC and E_d are calculated from the cloud droplet

164 spectrum data detected by FCDP. The calculation formulas are as follows:

165        $$Nc = \sum n_i \tag{1}$$

$$166 \qquad LWC = \sum \frac{4}{3} \pi r_i^3 \rho_w n_i \qquad (2)$$

$$167 \qquad E_d = 2 \frac{\sum n_i r_i^3}{\sum n_i r_i^2} \qquad (3)$$

168   In the formulas, n_i is the cloud number concentration for each bin. r_i is the median particle

169   size for each bin. ρ_w is the density of water.

170   Define the relative heights of the cloud as Zn:

$$171 \qquad Zn = \frac{Z - Z_{base}}{Z_{top} - Z_{base}} \qquad (4)$$

172   In the formula, Z_{base} is the height of the cloud base, and Z_{top} is the height of the cloud top. The

173   cloud heights have been normalized by setting the cloud base as 0 and the cloud top as 1.

174   Similar to previous studies, the first indirect effect of aerosol or Twomey effect of aerosols and

175   clouds is defined as:

$$176 \qquad FIE = -\left(\frac{\Delta \ln E_d}{\Delta \ln \alpha} \right)_{LWC} \qquad (5)$$

177   In the formula, α represents the physical quantity of aerosols, which can be quantified using

178   aerosol optical depth (Feingold et al., 2001), aerosol extinction coefficient (Feingold et al., 2003),

179   cloud condensation nuclei concentration, and aerosol number concentration (Che et al., 2021; Zhao

180   et al., 2012; Zhao et al., 2018). The FIE value may vary with the variables representing the aerosol

181   amount.

182   **2.2. Reanalyze data**

183   The vertical pressure velocity (Pa·s⁻¹) was obtained from MERRA2, with a spatial resolution

184   of 0.625° × 0.5° and 42 layers and a temporal resolution of 3 hours. The data from the first to the

185   twenty-third layers, corresponding to pressure altitudes from 1000 hPa to 200 hPa, were selected,

186   covering the maximum altitude of aircraft observations. An average calculation was performed to

187   obtain the vertical pressure velocity for the Guangxi region from 08:00 to 20:00 during the

188   observation period, reflecting the temporal variation characteristics of vertical airflow above the

189   region. This dataset has been used in several studies (Ge et al., 2021; Kennedy et al., 2011; Painemal

190   et al., 2021).

191   **3. Results and discussion**

3.1 Vertical distribution characteristics of cloud microphysical quantities

Based on the criteria of Nc $\geq$ 10 cm^{-3} and LWC $\geq$ 10^{-3} g·m^{-3}, aerosol, cloud droplet, and meteorological data were distinguished between inside and outside the cloud. The vertical averages were calculated at 10 m height intervals, resulting in the vertical distributions of physical quantities from 9 observation flights, covering a height range of 0-4000 m and ensuring consistent vertical resolution for each physical quantity. Subsequently, the average vertical distribution of physical quantities from the 9 observation flights was calculated, leading to the vertical distribution diagrams of each physical quantity during the observation period, as shown in Fig. 1. The average vertical profiles of Na (interstitial aerosol, aerosol particles too small to activate to cloud droplets), Na (out cloud) (Fig. 1a), cloud microphysical quantities (Fig. 1b) and meteorological elements (Fig. 1c-d) during the observation period was obtained. Na (interstitial aerosol) decreased gradually with height and was affected by aerosols in the atmospheric environment. Below 1500 m, Nc first decreased and then stabilized with increasing height, following a trend similar to that of Na. This indicates that the number of cloud condensation nuclei capable of activating cloud droplets diminishes as altitude increases. Compared to the upper atmosphere (above 1500 m), there were more cloud condensation nuclei in the lower atmosphere, resulting in an average Nc value of 407 cm^{-3}. Between 1500 m and 3300 m, Nc showed little variation with height, remaining concentrated around 100 cm^{-3} at each altitude (Fig.1a). The low Nc observed at certain altitudes may be due to the observation area being close to the edge of the cloud.
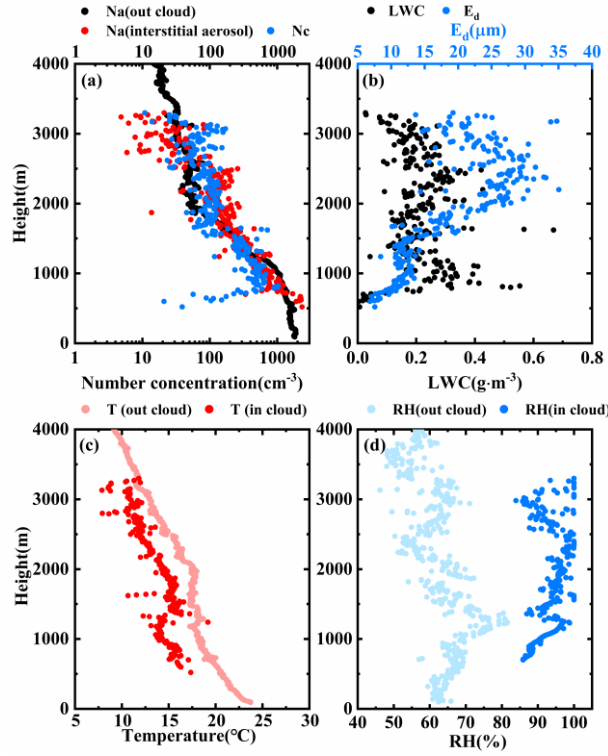
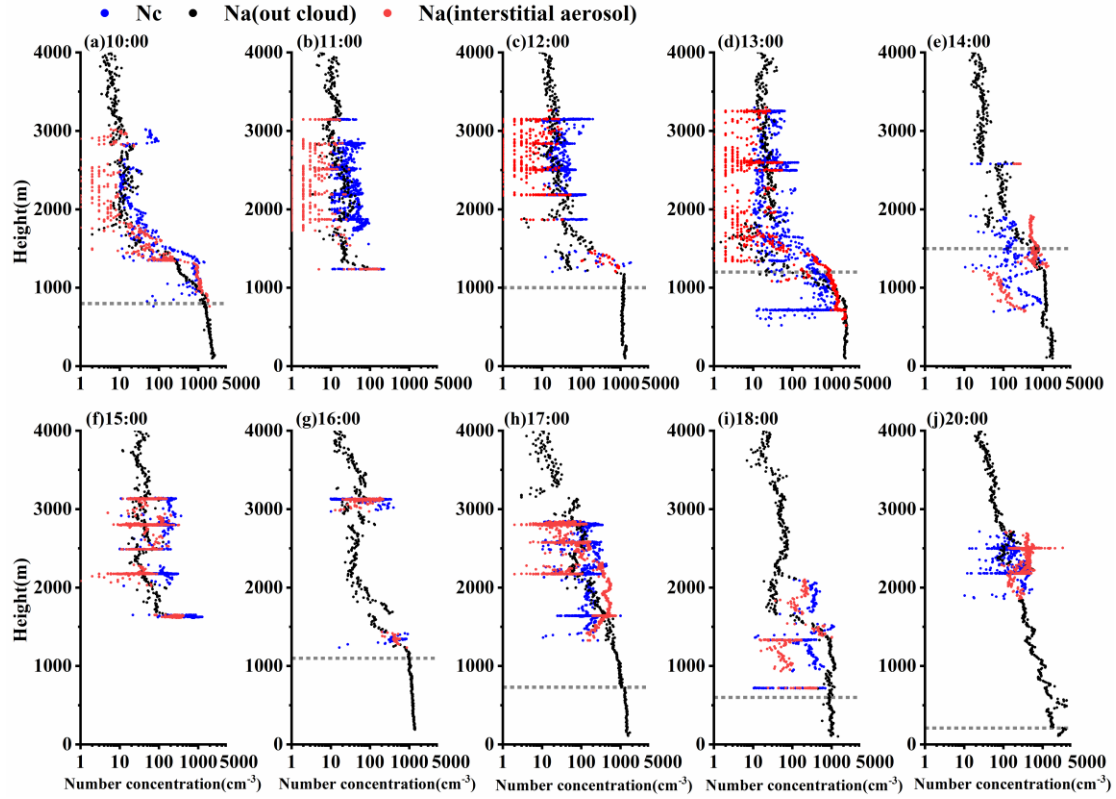**Fig. 1** Average vertical profiles of cloud interstitial aerosol concentration, outside aerosol number concentration, cloud droplet concentration (a), LWC, effective diameter of cloud droplet (b), temperature inside and outside cloud (c), and relative humidity inside and outside cloud (d) during the observation period

With the increase in height, E_d first increased, then remained unchanged and then increased (Fig. 1b). A large number of cloud droplets competed for water vapor below 1500 m, which is not conducive to the growth of cloud droplets, so the average E_d was only 11.21 μm. In Guangxi, the top of PBL during autumn ranges from 1000 to 1500 m (Fig.1c), where temperature inversion layers occur. This temperature structure increases the stability of the air, suppressing the formation of vertical airflow and hindering the growth of cloud droplets. Above 1500 m, Nc was lower than the near ground, and the lower atmospheric temperature was conducive to increasing cloud droplet particle size. The average value of E_d reached 22.78 μm. The value of LWC was independent of height, with an average value of 0.22 g·m^{-3} in Guangxi (Fig. 1b). RH is consistently above 60 %, making it likely for the air to reach saturation and lead to cloud formation.

3.2 Time variation of the vertical distribution of cloud microphysical quantities

Fig. 2 Vertical profiles of cloud interstitial aerosol concentration, outside aerosol number concentration, and cloud droplet concentration at different times (a is 10:00, b is 11:00, c is 12:00, d is 13:00, e is 14:00, f is 15:00, g is 16:00, h is 17:00, i is 18:00, j is 20:00, the black dashed line represents the height of PBL)

To understand the time variation of the vertical distribution of cloud microphysical quantities, the data were classified. Vertical profiles of interstitial aerosol (Na), Na outside the cloud (Fig. 2), cloud microphysical quantities (Fig. 3), and meteorological elements inside and outside the cloud (Fig. 4) were obtained at ten times from 10:00 to 18:00 and at 20:00. The data collected inside the cloud were original, while the average values outside the cloud were calculated at 10 m intervals.
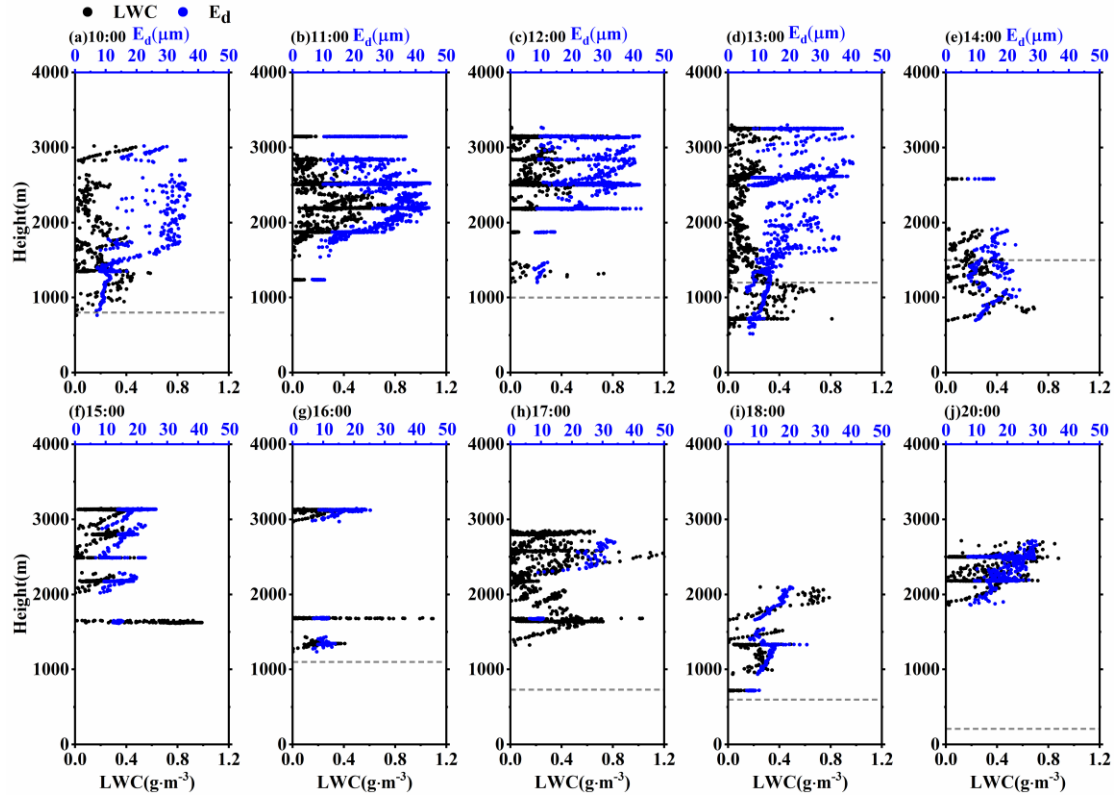
Fig. 3 Vertical profiles of liquid water content and effective diameter of cloud droplets at different times (a 10:00, b 11:00, c 12:00, d 13:00, e 14:00, f 15:00, g 16:00, h 17:00, i 18:00, j 20:00, the black dashed line represents the height of PBL)

At 10:00, N_c below 900 m was less than 100 cm^{-3}, and N_a in PBL was high (Fig. 2a). Although there were sufficient aerosols that can be activated into cloud condensation nuclei, RH > 60 %, the atmospheric temperature was high, which was not conducive to the activation of small-size aerosol particles (Fig. 3a). At the same time, LWC was low, and the condensed cloud droplets are difficult to grow, and the average E_d is only 8.01 μm (Fig. 3a). Between 900m and 1500 m, there were not only sufficient cloud condensation nuclei but also sufficient water vapor and temperature conditions, which are conducive to the formation of cloud droplets. The average N_c and E_d increased to 430 cm^{-3} and 11.15 μm. Above 1500 m, although the water vapor condition was sufficient (LWC = 0.16 g·m^{-3}), the cloud condensation nucleus was few, resulting in an average N_c value of only 35 cm^{-3}. However, sufficient LWC was conducive to the growth of cloud droplets, and E_d was significantly higher than clouds below 1500 m, with E_d ranging from 13.82 to 37.26 μm. At 1500 m, N_a (interstitial aerosol) was 34 cm^{-3}, increasing to 134 cm^{-3} at 1600 m. RH remained nearly constant in this range, while LWC rose from 0.16 to 0.19 g·m^{-3}, promoting the hygroscopic growth of aerosols. However, N_c did not show a significant increase. Thus, the temperature inversion layer (Fig. 4a) within the cloud may contribute to the rise in N_a (interstitial aerosol). This increase suggests more aerosols are inactive or unable to activate within the cloud. These aerosols may result from mixing warm air from outside the cloud at the cloud base (Lu et al., 2011). Furthermore, the temperature inversion layer may hinder vertical airflow within the cloud, suppressing cloud droplet growth.

At 11:00, aerosols were transported by updrafts (Fig. 5a) to around 1500 m (near the top of PBL) and activated into cloud condensation nuclei. Below 1500 m, the average N_c value was 102 cm^{-3} (Fig. 2b), while the average LWC value was only 0.03 g·m^{-3} (Fig. 3b). Cloud droplets were competing for water vapor. The E_d value was only 8.20 μm, similar to the cloud microphysical characteristics near the PBL at 10:00. Between 1500 m and 3150 m, N_a was less than 10 cm^{-3}, indicating insufficient CCN, and the average N_c was only 29 cm^{-3}. Compared to 10:00, the LWC was higher (mean 0.19 g·m^{-3}), resulting in a larger E_d in the upper part of the cloud, with an average of 28.95 μm.
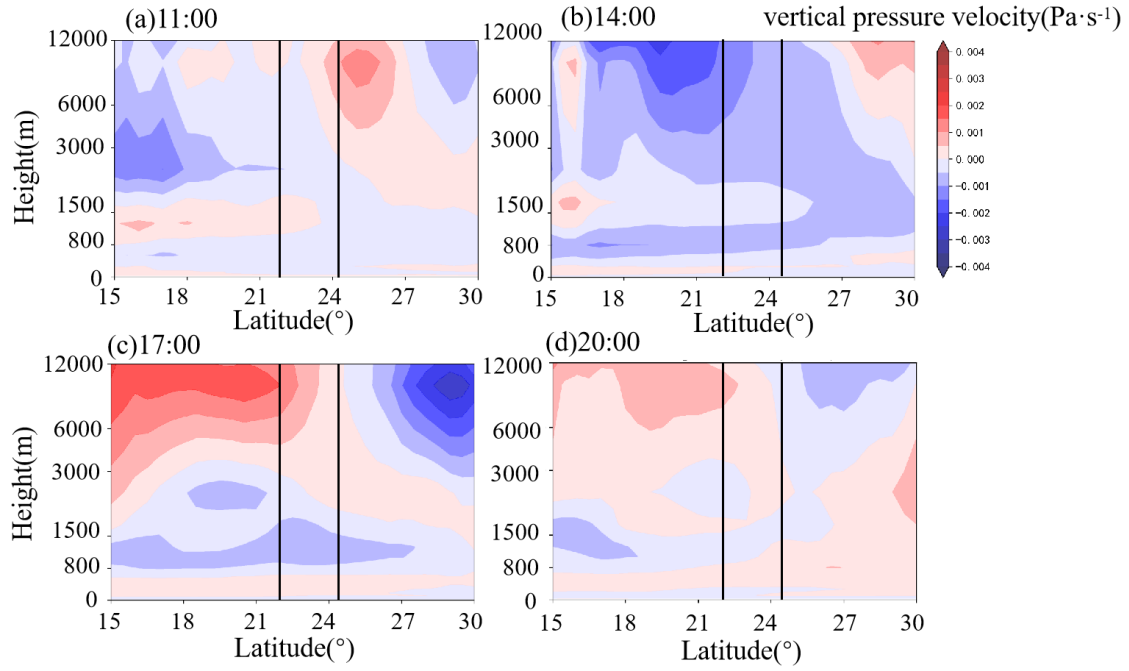
Fig 5 Latitudinal profiles of vertical pressure velocity at different times in Guangxi (solid black line is the latitude range observed by aircraft, and a positive value is downdraft, a negative value is updraft, a is 11:00, b is 14:00, c is 17:00, d is 20:00)

At 12:00, the height of PBL top rose to 1000 m, the near-surface aerosol was transported to 1200-1500 m (Fig. 2c, the mean value of Na outside the cloud was 578 cm^{-3}), the mean value of Nc reached 399 cm^{-3}, and the mean value of E_d was only 9.41 μm (Fig. 3c), higher than 11:00. Stratocumulus clouds above 1800 m had low Nc (mean 35 cm^{-3}) and large E_d (mean 26.14 μm).

At 13:00, the Nc ranged from 13 to 2052 cm^{-3} below 1200 m (Fig. 2d), which may be attributed to the uneven development of clouds within the detection range. The increase in solar radiation leads to high near-surface temperatures (Fig. 4d, T > 25 °C), which enhances turbulent activity within the PBL and is favorable for cloud droplet formation. Therefore, Nc at 13:00 was larger than that at 10:00, and many cloud droplets hindered their particle size growth, with an average E_d value of 9.23 μm (Fig. 3d). From 1200 m to 1500 m, the mean values of Nc and E_d were 155 cm^{-3} and 12.29 μm. At this height, a strong temperature inversion layer appeared (Fig. 4d), and cloud droplet evaporation activity was enhanced (Li et al., 2003), resulting in a higher Na (interstitial aerosol) than Na (out cloud). For Stratocumulus clouds above 1500 m, the Nc varied little with height, and the average E_d was 21.45 μm.

At 14:00, the Nc range below 1500 m was 11 to 1109 cm^{-3} (Fig. 2e), with the highest PBL top height at 1500 m, which diluted the Na (out of the cloud) within the PBL, resulting in a decrease in

291   the maximum Nc (Nc = 1109 cm^{-3}). The average LWC was 0.29 g·m^{-3} (Fig. 3e), higher than at 13:00,

292   providing moisture conditions for cloud droplet growth, while the upward airflow was strong (Fig.

293   5b). Consequently, the average E_d was 13.75 μm. A temperature inversion layer was present at 2500

294   m (Fig. 4e), hindering aerosol diffusion and enhancing the evaporation of cloud droplets near the

295   cloud top, leading to a peak in Na (interstitial aerosol) at that height.

296   At 15:00, the Nc and Na (interstitial aerosol) between 1600 m and 2000 m were higher than

297   those at 14:00 with average values of 720 cm^{-3} and 249 cm^{-3} (Fig. 2f). Due to the increase in Nc,

298   the average E_d was only 13.72 μm (Fig. 3f). The increase in Na (out cloud) above 2000 m provided

299   CCN, resulting in an average Nc of 146 cm^{-3}. Although the moisture conditions were sufficient, with

300   an average LWC of 0.23 g·m^{-3}, which was higher than the 0.05 g·m^{-3} recorded at 14:00 (Fig. 3f),

301   and RH was 52% (Fig. 4f), the average E_d decreased to 16.73 μm. This decrease was due to the

302   competition for moisture among cloud droplets, which led to an increase in small particle-size cloud

303   droplets.

304   At 16:00, Nc and Na (interstitial aerosol) below 2000 m were relatively large, 458 and 468 cm^{-}

305   ^{3}, respectively (Fig. 2g). The temperature inversion layer at the top of PBL hinders the condensation

306   growth of cloud droplets. The average E_d was only 11.00 μm (Fig. 3g). Similar to the observations

307   at 15:00, Na (out cloud) and Na (interstitial aerosol) near 3000 m were higher. The low temperature

308   (T = 7.75 °C) and high humidity (RH = 70 %) of the cloud environment (Fig. 4g) were conducive

309   to the activation of aerosol. The maximum value of Nc reached 395 cm^{-3}. However, the average of

310   E_d was only 17.13 μm due to water vapor contention between cloud droplets.

311   At 17:00, the height of PBL decreased to 730 m. Aerosols were transported above the PBL (Fig.

312   2h), providing CCN above 2000 m. Nc remained constant with an average of 134 cm^{-3} (Fig. 2h),

313   while E_d averaged 17.12 μm (Fig. 3h). Under the cooling of the atmosphere and the cooling of the

314   cloud tops at sunset, the E_d near the cloud tops is greater than 30 μm. The temperature inversion

315   layer of 1600-2000 m (Fig. 4h) enhanced cloud droplet growth and hindered aerosol diffusion,

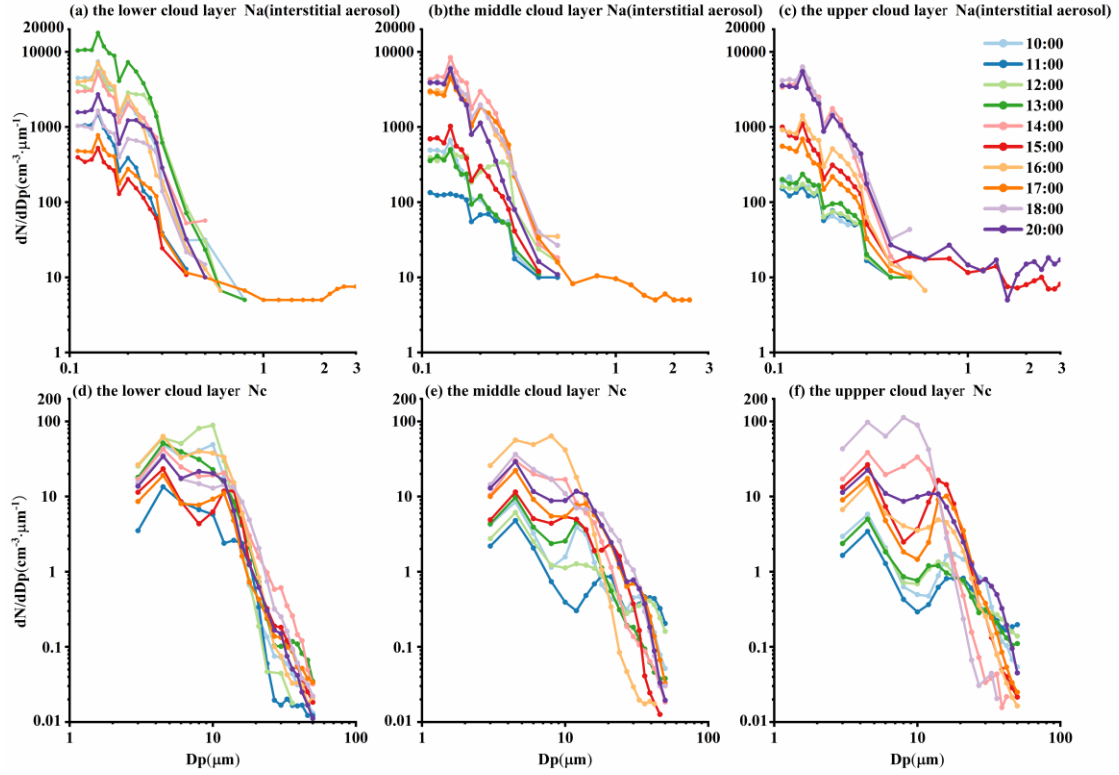316   causing the Na (interstitial aerosol) to be higher than the Na out cloud.

Fig 6 Cloud interstitial aerosol number concentration spectrum and cloud droplet number concentration spectrum (a-c is the aerosol spectrum of lower cloud, middle cloud and upper cloud, and d-f is the cloud droplet spectrum of lower cloud, middle cloud and upper cloud, respectively)

At 18:00, the height of PBL decreased to 500 m, resulting in the accumulation of aerosols between 900 m and 1400 m (Fig. 2i), which led to the formation of small particle-size cloud droplets, with an average Nc of 273 cm^{-3} and an average E_d of 16.67 μm (Fig. 3i). Similar to the observations at 17:00, the atmospheric temperature above 1400 m was high (Fig. 4i), and cloud droplet evaporation caused Na (interstitial aerosol) to be close to or greater than Na (out cloud).

At 20:00, there were upward flows between 1000 and 1500 m (Fig. 5d). The abundance of CCN and low temperature (Fig. 4j) promoted the formation and growth of cloud droplets. The average Nc was 194 cm^{-3} (Fig. 2j), higher than the Nc observed from 10:00 to 13:00. LWC and Ed gradually increased with height (Fig 3j). LWC rose from 0.02 $g·m^{-3}$ to 0.64 $g·m^{-3}$. Ed increased from 7.52 μm to 29.59 μm.

The cloud height is normalized, and the relative height of the cloud is set as Zn ($0 ≤ Zn ≤ 1$). $Zn < 0.33$ is the lower cloud layer, $0.33 ≤ Zn < 0.67$ is the middle cloud layer, and $Zn ≥ 0.67$ is the upper cloud layer. The concentration spectra of cloud interstitial aerosol numbers (Fig. 6a-c) and cloud droplet numbers (Fig. 6d-f) at different locations at different times were obtained.

From 10:00 to 13:00, the interstitial aerosol particle size in the cloud's lower layer was

336 concentrated below 0.4 μm. In comparison, the cloud droplet diameter was primarily concentrated

337 below 20 μm, with few large particle-size cloud droplets (Fig. 6a,6d). In the middle cloud layer, Na

338 across all particle size ranges had decreased to below 1000 $cm^{-3} \cdot \mu m^{-1}$. Nc for particles smaller than

339 20 μm has decreased, while Nc for particles larger than 20 μm exceeded 0.1 $cm^{-3} \cdot \mu m^{-1}$(Fig. 6b, 6e).

340 Na in the upper cloud layer was minimal compared to the middle and lower layers. Sufficient water

341 vapor (LWC = 0.14 $g \cdot m^{-3}$, Fig.3a-c) and low temperature (T = 11.72 ℃, Fig.4a-c) promote the

342 growth of cloud droplets, resulting in fewer Nc for particles larger than 20 μm in the upper layer

343 (Fig. 6c, 6f) compared to the middle layer.

344 From 14:00 to 16:00, aerosols diffused upward with the increase in PBL, leading to a decrease

345 in Na in the cloud's lower layer (Fig. 6a,6d). The upward transport of aerosols caused the upper-

346 level Na of the cloud to be higher than that observed from 10:00 to 13:00. This change increased

347 the Nc of droplets with diameters greater than 20 μm (Fig. 6b-c, 6e-f). Newly formed cloud droplets

348 competed for water vapor. Nc of droplets larger than 30 μm decreased, while Nc of smaller droplets

349 increased.

350 From 17:00 to 20:00, the height of PBL decreased. Na increased, and Nc of large droplets

351 decreased. Aerosols retained at the top of PBL provided CCN for the cloud's middle and upper layers

352 (Fig. 6b-c, 6e-f). During this period, Nc was higher than observed from 10:00 to 13:00. The increase

353 in Nc may be attributed to the rise in Nc of droplets smaller than 20 μm.

354 **3.3 Verification of the Twomey Effect**

355 Previous studies have shown two sources of aerosols in Guangxi, namely the land and the

356 ocean, where air masses from land will bring higher aerosol particle number concentrations (Liu et

357 al., 2024). According to the classification of air mass sources, the frequency distributions of Na

358 (interstitial aerosol), Nc, LWC and E_d under the influence of land and ocean air masses were
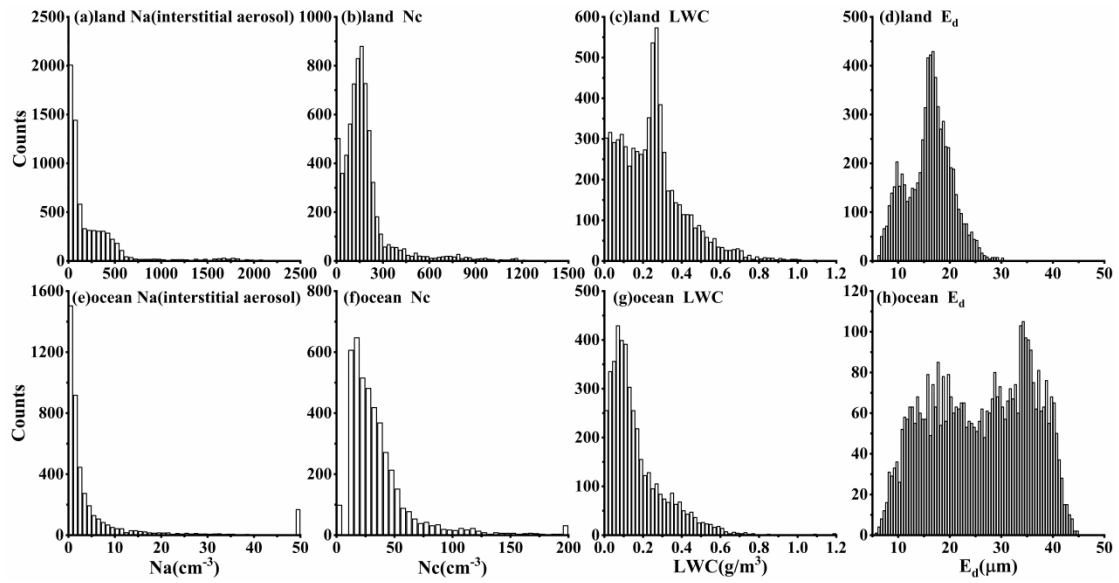
359 obtained (Fig. 7).

Fig. 7 The distributions of cloud interstitial aerosol number concentration (a and e), cloud droplet number concentration (b and f), LWC (c and g) and cloud droplet effective diameter (d and h) under different air mass sources, the y-axis represents the number of samples.

Under the influence of land air mass, Na (interstitial aerosol) was less than 500 cm^{-3}, and Nc was high. The frequency distribution of E_d was unimodal, mainly concentrated in the range of 16-18 μm (Fig. 7a). Under the influence of ocean air mass, Na (interstitial aerosol) was mainly less than 20 cm^{-3}. Nc was primarily distributed in the range of 10 to 50 cm^{-3}. E_d was significantly higher than that under the influence of land air mass. E_d presented a bimodal distribution with peak values of 17.75 and 34.25 μm (Fig. 7b).

In addition to the influence of the air mass source, the vertical distribution of Na is also affected by PBL. We selected two aircraft observation data on October 29 and November 02 to analyze the influence of PBL on the cloud microphysical quantities. The observed cloud base height was lower than the heights of PBL, and the cloud top height was > 1500 m. The clouds crossed the top of PBL, and the cloud thickness was similar (about 2500 m).

According to the vertical profiles of the aerosol number concentration spectrum (Fig. 8a-b), there were significant differences between the two Na profiles. In the height affected by the PBL (below 1500 m), aerosol pollution occurred on October 29 (Na > 1000 cm^{-3}), and the atmosphere was clean on November 2 (Na < 600 cm^{-3}). In the upper atmosphere (above 1500 m), aerosol pollution (Na < 200 cm^{-3}) occurred on November 2 compared to October 29 (Na < 100 cm^{-3}).
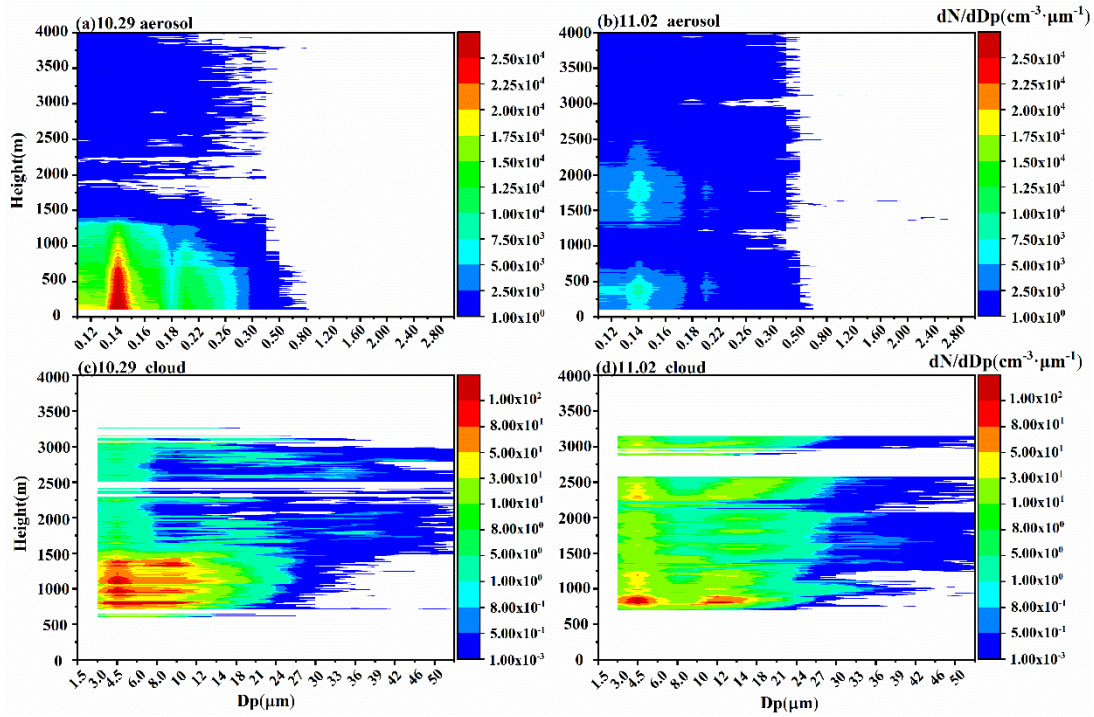
Fig. 8 Vertical profiles of aerosol number concentration spectra (a and b) and cloud droplet number concentration spectra (c and d) on 29 October and 2 November

On October 29, the aerosol pollution in PBL was severe (Fig.9a, N_a = 1331 cm^{-3}). The aerosol number concentration spectrum exhibited a bimodal distribution, with peak diameters of 0.14 and 0.22 μm (Fig.8a). The atmosphere contained sufficient CCN, resulting in a large N_c (Fig.9a, N_c = 460 cm^{-3}). As shown in the cloud droplet number concentration spectrum (Fig. 8c), most cloud droplets were concentrated in the size range of 3-24 μm (Fig.8c). E_d was 9.69 μm (Fig. 9e), primarily because many cloud droplets competed for water vapor, making it difficult for them to grow into larger droplets. A strong inversion layer at 1500 m (Fig.9c) hindered the upward transport of aerosols. Consequently, N_a above 1500 m was low, leading to a reduced N_c, with an average of only 35 cm^{-3}. Fig. 8c showed that cloud droplet sizes within the PBL primarily range from 8 to 21 μm. In contrast, above the PBL, cloud droplet sizes are mainly distributed below 8 μm and above 21 μm, with an average effective diameter (E_d) of 25.28 μm (Fig. 9e). These large particle-size cloud droplets likely originated from the collision and growth of droplets within the 8.0 to 21 μm range.
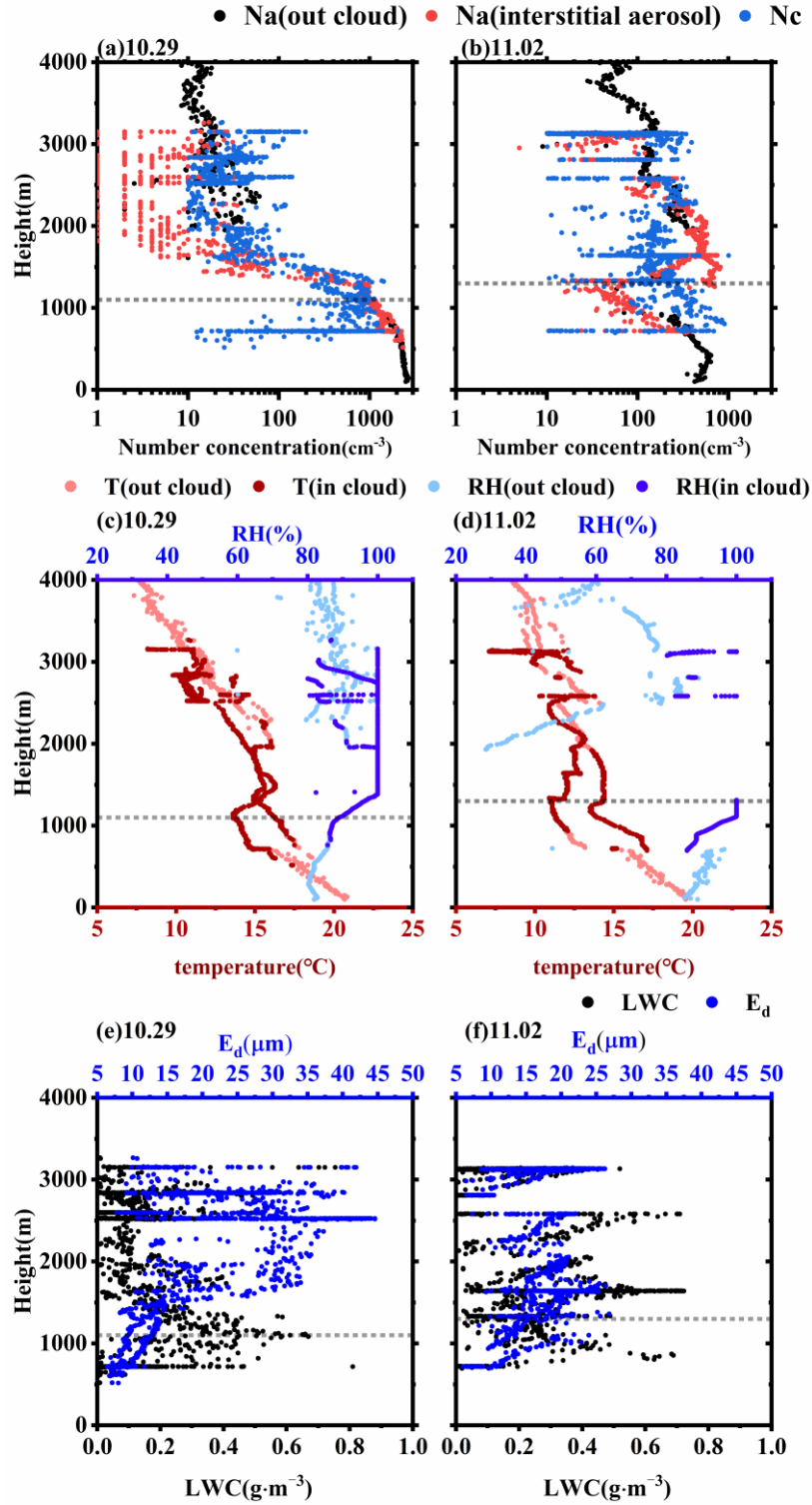
Fig. 9 Vertical profiles of outside aerosol concentration, cloud intercloud aerosol concentration, cloud droplet concentration (a and b), temperature inside and outside the cloud, relative humidity inside and outside the cloud (c and d), LWC, and effective droplet diameters (e and f) on October 29 and November 2, the black dashed line represents the height of PBL.

On November 2, Na in PBL (Fig. 9b, Na = 405 cm^{-3}) was slightly higher than Na in the upper air (Na = 220 cm^{-3}). The Nc in PBL (Nc = 243 cm^{-3}) was higher than that above PBL (Nc = 124 cm^{-}

^{3}). The concentration spectra of cloud droplet numbers exhibited a bimodal distribution (Fig. 8d). The presence of a large number of small cloud droplets in the PBL hinders the growth of larger droplets, resulting in a lower number of large cloud droplets (Dp > 18 μm) in the PBL compared to the upper air. E_d in PBL (Fig. 9f, E_d = 12.89 μm) was lower than in the upper air (E_d = 17.94 μm). The inversion layer (Fig.9d, about 750 m in thickness) above the top of PBL enhanced the evaporation activity of cloud droplets, leading to a lower Nc at this height compared to other heights and a higher Na (interstitial aerosol) than that observed at other heights.
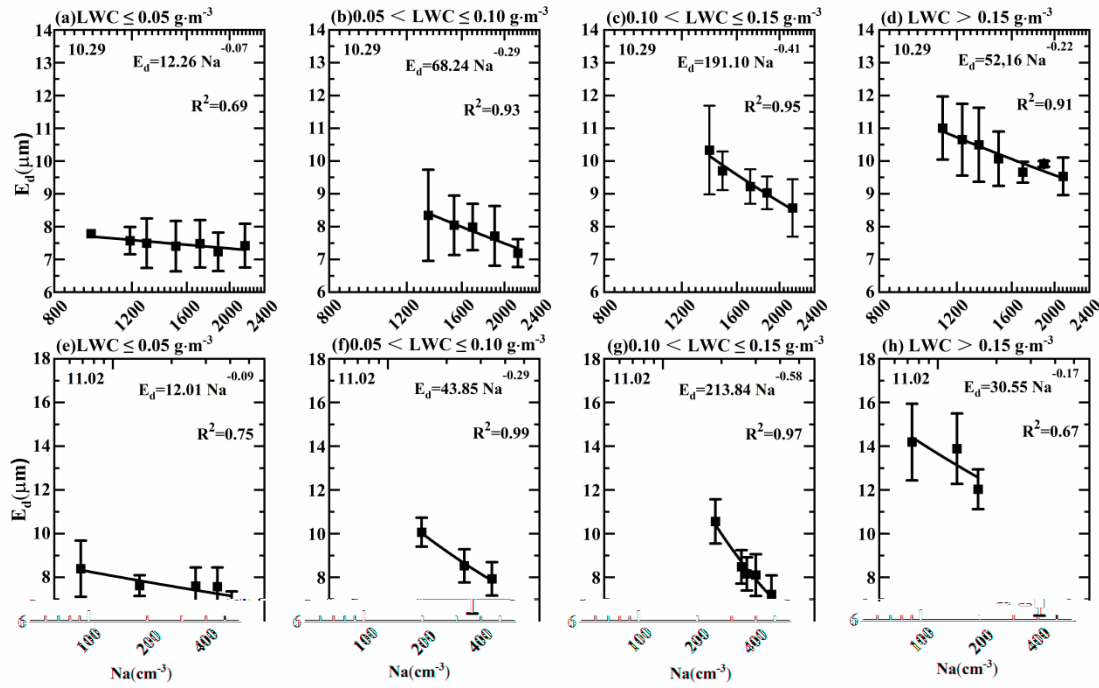

Fig. 10 Correlation between aerosol number concentration and effective droplet diameter in the range of 0-0.05, 0.05-0.10, 0.10-0.15 and > 0.15 g·m^{-3} LWC (a-d are October 29, e-f are November 2, R^2 is the correlation coefficient. The significance level α was set at 0.05, and the P-value < 0.05 was obtained.)

To understand whether the relationship between aerosol and cloud in Guangxi is consistent with the Twomey effect, we classified the in-cloud data below 1000 m on October 29 and November 2. We calculated the FIE index of LWC in different ranges (Fig. 10). The equation in the panel represented a fitted curve for the data, indicating the relationship between Na and E_d. The relationship between Na and E_d can be expressed as $E_d = Na^{FIE}$. The results showed that Na and E_d were always negatively correlated regardless of low LWC condition or high LWC condition. Therefore, the relationship between aerosol and stratocumulus in Guangxi is consistent with the Twomey effect, and E_d decreases with the increase of Na.

4. Conclusion

422   This study provides the vertical profiles of stratocumulus microphysical quantities, number

423   concentration spectrum and meteorological parameters over Guangxi in autumn using the aircraft

424   observation data of 9 sorties. The daylight variation of cloud microphysical characteristics at

425   different altitudes are described, and the effects of air mass source on cloud microphysical quantities

426   are discussed. The results are as follows.

427   (1) Below 1500 m in Guangxi, Na and Nc gradually decreased with the increase in altitude.

428   Aerosols were mainly concentrated under PBL. Nc was large, with an average of 407 cm^{-3}. Between

429   1500 m and 3300 m, the value of Na remained low, with Nc staying below 200 cm^{-3} and not changing

430   with height. With the increase in height, E_d first increased, then remained constant, and finally

431   increased again. The E_d at the cloud top was 2.75 times that at the cloud base. The inversion layer

432   at the top of PBL hindered the increase in the cloud droplet particle size. Compared with other

433   regions in China, LWC was high, with an average value of 0.22 g·m^{-3}, and LWC variation was

434   independent of height.

435   (2) The vertical distribution of microphysical quantities of stratocumulus in autumn in this

436   region had noticeable daylight variation, mainly influenced by the daylight variation of the vertical

437   distribution of aerosols. From 10:00 to 13:00, aerosols were primarily concentrated at low altitudes,

438   which led to smaller particle-size cloud droplets in the lower cloud layer (Nc = 313 cm^{-3}, E_d = 10.78

439   μm). From 14:00 to 16:00, due to the combined effects of the lifting of the top of the PBL and

440   updrafts, the low-level aerosols were diluted, leading to a decrease in the number of cloud droplets

441   in the lower layer (Nc = 184 cm^{-3}). From 17:00 to 20:00, the descending motion and downdrafts of

442   the PBL increased the number of small cloud droplets in the lower layer (E_d = 12.15 μm). From

443   10:00 to 13:00, Nc in the middle and upper clouds was low, while the particle size was large. From

444   14:00 to 20:00, the upward transport of aerosols near the surface and the formation of a high

445   concentration aerosol layer (600-1300 m) increased the number of small particle-size cloud droplets

446   in the middle and upper clouds.

447   (3) The air mass source and PBL influenced the distribution characteristics of cloud

448   microphysical quantities by influencing Na. Nc under the influence of the land air mass was 5.06

449   times that of the ocean air mass, while E_d under the influence was 1.62 times that of the land air

450   mass. When there was a high number concentration of aerosols below PBL, the cloud droplet

451   number concentration spectrum was unimodal, and the cloud droplet size was concentrated below

20 μm. Above PBL, the cloud droplet number concentration spectrum was bimodal, and the number of large particle-size cloud droplets (cloud droplet diameter > 30 μm) was more than that in PBL. The relationship between aerosol and cloud in the Guangxi region was consistent with the Twomey effect. E_d and Na were negatively correlated in different LWC ranges, and FIE ranged from -0.07 to -0.58.

In conclusion, our findings highlight the significant influence of aerosol concentrations and air mass origins on the microphysical properties of stratocumulus clouds over Guangxi. The observed daylight and vertical variations in cloud microphysics underscore the complexity of aerosol-cloud interactions in this region. Future research should cover a comprehensive time frame, including nighttime observations, to provide a complete vertical structure of these clouds, the effects of different aerosol types, and their impact on regional climate patterns.

References

Albrecht, B. A.: Aerosols, cloud microphysics, and fractional cloudiness, Science, 245(4923), 1227-1230, https://doi.org/10.1126/science.245.4923.1227, 1989.

Almeida, G. P., Brito, J., Morales, C. A., Andrade, M. F., and Artaxo, P.: Measured and modelled cloud condensation nuclei (CCN) concentration in São Paulo, Brazil: the importance of aerosol size-resolved chemical composition on CCN concentration prediction, Atmos. Chem. Phys., 14, 7559-7572, https://doi.org/10.5194/acp-14-7559-2014, 2014.

Betts, A. K.: Coupling of water vapor convergence, clouds, precipitation, and land-surface processes, J. Geophys. Res-atmos., 112, D10108, https://doi.org/10.1029/2006JD008191, 2007.

Bosilovich, M. G., Akella, S., Coy, L., Cullather, R., Draper, C., Gelaro, R., Kovach, R., Liu, Q., Molod, A., Norris, P., Wargan, K., Chao, W., Reichle, R., Takacs, L., Vikhliaev, Y., Bloom, S., Collow, A., Firth, S., Labow, G., Partyka, G., Pawson, S., Reale, O., Schubert, S. D., Suarez, M., and Global Modeling and Assimilation Office (GMAO): MERRA-2, Greenbelt, MD, USA, Goddard Earth Sciences Data and Information Services Center (GES DISC), https://disc.gsfc.nasa.gov/daac-bin/FTPSubset2.pl (last access: 7 January 2024), 2015.

Che, Y., Zhang, J., Fang, C., Zhou, X., Xue, W., Hu, X., Duan, J., Li, W., Gao, Y., Lu, G., Zhao, D., Zhao, C.: Aerosol and cloud properties over a coastal area from aircraft observations in Zhejiang, China, Atmos. Environ., 267, 118771, https://doi.org/10.1016/j.atmosenv.2021.118771, 2021.

Chen, Y., Wang, S., Min, Q., Lu, S., Lin, P., Lin, N., Chung, K., Joseph, E.: Aerosol impacts on warm-cloud microphysics and drizzle in a moderately polluted environment, Atmos. Chem. Phys., 21(6), 4487–4502. https://doi.org/10.5194/acp-21-4487-2021, 2021.

Collaud Coen, M., Weingartner, E., Apituley, A., Ceburnis, D., Fierz-Schmidhauser, R., Flentje, H., Henzing, J. S., Jennings, S. G., Moerman, M., Petzold, A., Schmid, O., Baltensperger, U.: Minimizing light absorption measurement artifacts of the Aethalometer: evaluation of five correction algorithms, Atmos. Meas. Tech., 3(2), 457-474, https://doi.org/10.5194/amt-3-

457-2010, 2010.

De, Boer G., Tripoli, G J., Eloranta, E W.: Preliminary comparison of CloudSAT-derived microphysical quantities with ground-based measurements for mixed-phase cloud research in the Arctic, J. Geophys. Res-atmos., 113, D00A06, https://doi.org/10.1029/2008JD010029, 2008.

Dusek, U., Frank, G. P., Hildebrandt, L., Curtius, J., Schneider, J., Walter, S., Chand, D., Drewnick, F., Hings, S., Jung, D., Borrmann, S., Andreae, M. O.: Size matters more than chemistry for cloud-nucleating ability of aerosol particles, Science, 312(5778), 1375-1378, https://doi.org/10.1126/science.1125261, 2006.

Feingold, G., Remer, L. A., Ramaprasad, J., Kaufman, Y. J.: Analysis of smoke impact on clouds in Brazilian biomass burning regions: An extension of Twomey's approach, J. Geophys. Res-atmos., 106(D19), 22907-22922, https://doi.org/10.1029/2001JD000732, 2001.

Feingold, G., Eberhard, W. L., Veron, D. E., Previdi, M.: First measurements of the Twomey indirect effect using ground-based remote sensors, Geophys. Res. Lett., 30(6), 1287, https://doi.org/10.1029/2002GL016633, 2003.

Ferek, R. J., Hegg, D. A., Hobbs, P. V., Durkee, P., Nielsen, K.: Measurements of ship-induced tracks in clouds off the Washington coast, J. Geophys. Res-atmos., 103(D18), 23199-23206, https://doi.org/10.1029/98JD02121, 1998.

Ge, J., Wang, Z., Wang, C., Yang, X., Dong, Z., Wang, M.: Diurnal variations of global clouds observed from the CATS spaceborne lidar and their links to large-scale meteorological factors, Clim. Dynam., 57, 2637-2651. https://doi.org/10.1007/s00382-021-05829-2, 2021.

Gunthe, S. S., King, S. M., Rose, D., Chen, Q., Roldin, P., Farmer, D. K., Jimenez, J. L., Artaxo, P., Andreae, M. O., Martin, S. T., and Pöschl, U.: Cloud condensation nuclei in pristine tropical rainforest air of Amazonia: size-resolved measurements and modeling of atmospheric aerosol composition and CCN activity, Atmos. Chem. Phys., 9(19), 7551-7575, https://doi.org/10.5194/acp-9-7551-2009, 2009.

Han, Q., Rossow, W. B., & Lacis, A. A.: Near-global survey of effective droplet radii in liquid water clouds using ISCCP data, J. Climate., 7(4), 465-497, https://doi.org/10.1175/1520-0442(1994)007%3C0465:NGSOED%3E2.0.CO;2, 1994.

Harikishan, G., Padmakumari, B., Maheskumar, R. S., Pandithurai, G., Min, Q. L.: Aerosol indirect

542   effects from ground-based retrievals over the rain shadow region in Indian subcontinent, J.

543   Geophys. Res-atmos., 121(5), 2369-2382, https://doi.org/10.1002/2015JD024577, 2016.

544 Jose, S., Nair, V. S., Babu, S. S.: Anthropogenic emissions from South Asia reverses the aerosol

545   indirect effect over the northern Indian Ocean. Sci. Rep., 10(1), 18360,

546   https://doi.org/10.1038/s41598-020-74897-x, 2020.

547 Kennedy, A. D., Dong, X., Xi, B., Xie, S., Zhang, Y., Chen, J.: A comparison of MERRA and NARR

548   reanalyses with the DOE ARM SGP data, J. Clim., 24(17), 4541-4557,

549   https://doi.org/10.1175/2011JCLI3978.1, 2001.

550 Kim, B. G., Schwartz, S. E., Miller, M. A., Min, Q.: Effective radius of cloud droplets by ground-

551   based remote sensing: Relationship to aerosol, J. Geophys. Res-atmos., 108(D23), 4740,

552   https://doi.org/10.1029/2003JD003721, 2003.

553 Kim, S. W., Yoon, S. C., Won, J. G., Choi, S. C.: Ground-based remote sensing measurements of

554   aerosol and ozone in an urban area: A case study of mixing height evolution and its effect

555   on ground-level ozone concentrations, Atmos. Environ., 41(33), 7069-7081,

556   http://doi.org/10.1016/j.atmosenv.2007.04.063, 2007.

557 King, M. D., Platnick, S., Menzel, W. P., Ackerman, S. A., Hubanks, P. A.: Spatial and temporal

558   distribution of clouds observed by MODIS onboard the Terra and Aqua satellites, IEEE

559   Trans.   Geosci.   Remote   Sens.,   51(7),   3826-3852,

560   https://doi.org/10.1109/TGRS.2012.2227333, 2013.

561 Kleinman, L. I., Daum, P. H., Lee, Y.-N., Lewis, E. R., Sedlacek III, A. J., Senum, G. I., Springston,

562   S. R., Wang, J., Hubbe, J., Jayne, J., Min, Q., Yum, S. S., and Allen, G.: Aerosol

563   concentration and size distribution measured below, in, and above cloud from the DOE G-

564   1 during VOCALS-REx, Atmos. Chem. Phys., 12(1), 207-223, https://doi.org/10.5194/acp-

565   12-207-2012, 2012.

566 Koren, I., Kaufman, Y. J., Rosenfeld, D., Remer, L. A., Rudich, Y.: Aerosol invigoration and

567   restructuring of Atlantic convective clouds, Geophys. Res. Lett., 32, 14828,

568   https://doi.org/10.1029/2005GL023187, 2005.

569 Lance, S., Nenes, A., Rissman, T. A.: Chemical and dynamical effects on cloud droplet number:

570   Implications for estimates of the aerosol indirect effect, J. Geophys. Res-atmos., 109(D22),

571   https://doi.org/10.1029/2004JD004596, 2004.

572 Li, J., Li, P., Ren, G., Yuan, L., Li, Y., Yang, J.: Aircraft measurements of aerosol distribution, warm
573   cloud microphysical properties, and their relationship over the Eastern Loess Plateau in
574   China, Tellus B: Chem. Phys. Meteorol., 71(1), 1663994,
575   https://doi.org/10.1080/16000889.2019.1663994, 2019.

576 Li, Z., Li, R., Li, B.：Analyses on Vertical Microphysical Characteristics of Autumn Stratiform
577   Cloud in Lanzhou Region, Plateau. Meteorol., 22(6), 583-589,
578   http://dx.chinadoi.cn/10.3321/j.issn:1000-0534.2003.06.008, 2003.

579 Liu, S., Wang, H., Zhao, D., Ke, Y., Wu, Z., Shen, L., Zhao, T.: Aircraft observations of aerosols and
580   BC in autumn over Guangxi Province, China: Diurnal variation, vertical distribution and
581   source appointment, Sci. Total. Environ., 906, 167550,
582   https://doi.org/10.1016/j.scitotenv.2023.167550, 2004.

583 Liu, T., Liu, Q., Chen, Y., Wang, W., Zhang, H., Li, D., Sheng, J.: Effect of aerosols on the macro-
584   and micro-physical properties of warm clouds in the Beijing-Tianjin-Hebei region, Sci.
585   Total. Environ., 720, 137618, https://doi.org/10.1016/j.scitotenv.2020.137618 , 2020.

586 Lu, C., Liu, Y., & Niu, S.: Examination of turbulent entrainment-mixing mechanisms using a
587   combined approach, J. Geophys. Res-atmos., 116(D20),
588   https://doi.org/10.1029/2011JD015944, 2011.

589 Lu, M. L., Conant, W. C., Jonsson, H. H., Varutbangkul, V., Flagan, R. C., Seinfeld, J. H.: The
590   marine stratus/stratocumulus experiment (MASE): Aerosol-cloud relationships in marine
591   stratocumulus, J. Geophys. Res-atmos., 112, D10209,
592   https://doi.org/10.1029/2006JD007985, 2007.

593 Lu, Z., Liu, X., Zhang, Z., Zhao, C., Meyer, K., Rajapakshe, C., Wu, C., Yang, Z., Penner, J. E.
594   Biomass smoke from southern Africa can significantly enhance the brightness of
595   stratocumulus over the southeastern Atlantic Ocean, PNAS, 115(12), 2924-2929,
596   https://doi.org/10.1073/pnas.1713703115, 2018.

597 McFarquhar, G. M., Bretherton, C. S., Marchand, R., Protat, A., DeMott, P. J., Alexander, S. P.,
598   Roberts, G. C., Twohy, C. H., Toohey, D., Siems, S., Huang, Y., Wood, R., Rauber, R. M.,
599   Lasher-Trapp, S., Jensen, J., Stith, J. L., Mace, J., Um, J. U., Järvinen, E., Schnaiter, M.,
600   Gettelman, A., Sanchez, K. J., McCluskey, C. S., Russell, L. M., McCoy, I. L., Atlas, R. L.,
601   Bardeen, C. G., Moore, K. A., Hill, T. C. J., Humphries, R. S., Keywood, M. D., Ristovski,

602   Z., Cravigan, L., Schofield, R., Fairall, C., Mallet, M. D., Kreidenweis, S. M., Rainwater,

603   B., Alessandro, J. D., Wang, Y., Wu, W., Saliba, G., Levin, E. T., Ding, S., Lang, F, Truong,

604   S. H., Wolff, C., Haggerty, J., Harvey, M. J., Klekociuk, A. R., McDonald, A. Observations

605   of clouds, aerosols, precipitation, and surface radiation over the Southern Ocean: An

606   overview of CAPRICORN, MARCUS, MICRE, and SOCRATES, Bull. Am. Meteorol.

607   Soc., 102(4), E894-E928, https://doi.org/10.1175/BAMS-D-20-0132.1, 2021.

608   Miles, N. L., Verlinde, J., Clothiaux, E. E.: Cloud droplet size distributions in low-level stratiform

609   clouds, J. Atmos. Sci., 57(2), 295-311, https://doi.org/10.1175/1520-

610   0469(2000)057%3C0295:CDSDIL%3E2.0.CO;2, 2000.

611   Nakajima, T. Y., Uchiyama, A., Takamura, T., Tsujioka, N., Takemura, T., Nakajima, T.:

612   Comparisons of warm cloud properties obtained from satellite, ground, and aircraft

613   measurements during APEX intensive observation period in 2000 and 2001, J. Meteorol.

614   Soc. Jpn., Ser. II, 83(6), 1085-1095, https://doi.org/10.2151/jmsj.83.1085, 2005.

615   Painemal, D., Corral, A. F., Sorooshian, A., Brunke, M. A., Chellappan, S., Afzali Gorooh, V., Ham,

616   S. H., O'Neill, L., Smith Jr, W. L., Tselioudis, G., Wang, H., Zeng, X., Zuidema, P.: An

617   overview of atmospheric features over the Western North Atlantic Ocean and North

618   American East Coast-Part 2: Circulation, boundary layer, and clouds, J. Geophys. Res-

619   atmos., 126(6), e2020JD033423, https://doi.org/10.1029/2020JD033423, 2021.

620   Painemal, D., Kato, S., Minnis, P.: Boundary layer regulation in the southeast Atlantic cloud

621   microphysics during the biomass burning season as seen by the A-train satellite

622   constellation, J. Geophys. Res-atmos., 119(19), 11288-211302,

623   https://doi.org/10.1002/2014JD022182, 2014.

624   Pyrina, M., Hatzianastassiou, N., Matsoukas, C., Fotiadi, A., Papadimas, C. D., Pavlakis, K. G.,

625   Vardavas, I.: Cloud effects on the solar and thermal radiation budgets of the Mediterranean

626   basin, Atmos. Res., 152, 14-28, https://doi.org/10.1016/j.atmosres.2013.11.009, 2015.

627   Ramanathan, V. L. R. D., Cess, R. D., Harrison, E. F., Minnis, P., Barkstrom, B. R., Ahmad, E.,

628   Hartmann, D.: Cloud-radiative forcing and climate: Results from the Earth Radiation

629   Budget Experiment. Science, 243(4887), 57-63,

630   https://doi.org/10.1126/science.243.4887.57, 1989.

631   Rosenfeld, D., Andreae, M. O., Asmi, A., Chin, M., de Leeuw, G., Donovan, D. P., Kahn, R., Kinne,

632   S., Kivekäs, N., Kulmala, M., Lau, W., Schmidt, K. S., Suni, T, Wagner, T., Wild, M, Quaas,

633   J.: Global observations of aerosol-cloud-precipitation-climate interactions, Rev. Geophys.,

634   52(4), 750-808, https://doi.org/10.1002/2013RG000441, 2014.

635 Strapp, J. W., Leaitch, W., Liu, P.: Hydrated and dried aerosol-size-distribution measurements from

636   the particle measuring systems FSSP-300 probe and the deiced PCASP-100X probe, J.

637   Atmos. Oceanic. Technol., 9(5), 548-555, https://doi.org/10.1175/1520-

638   0426(1992)009%3C0548:HADASD%3E2.0.CO;2, 1992.

639 Su, T., Li, J., Li, C., Xiang, P., Lau, A. K. H., Guo, J., Yang, D., Miao, Y.: An intercomparison of

640   long-term planetary boundary layer heights retrieved from CALIPSO, ground-based lidar,

641   and radiosonde measurements over Hong Kong, J. Geophys. Res-atmos., 122(7), 3929-

642   3943, http://doi.org/10.1002/2016JD025937, 2017.

643 Terai, C. R., Bretherton, C. S., Wood, R., Painter, G.: Aircraft observations of aerosol, cloud,

644   precipitation, and boundary layer properties in pockets of open cells over the southeast

645   Pacific,   Atmos. Chem. Phys., 14(15), 8071-8088, https://doi.org/10.5194/acp-14-8071-

646   2014, 2014.

647 Twomey, S.: The influence of pollution on the shortwave albedo of clouds, J. Atmos. Sci., 34(7),

648   1149-1152, https://doi.org/10.1175/15200469(1977)034%3C1149:TIOPOT%3E2.0.CO;2,

649   1977.

650 Waliser, D. E., Li, J. L., L'Ecuyer, T. S., Chen, W. T.: The impact of precipitating ice and snow on

651   the radiation balance in global climate models, Geophys. Res. Lett., 38(6), L06802,

652   https://doi.org/10.1029/2010GL046478, 2011.

653 Wang, H. Data for Aircraft observations of aerosol and microphysical quantities of stratocumulus

654   in autumn over Guangxi Province, China: Diurnal variation, vertical distribution and

655   aerosol-cloud relationship [Data set]. Zenodo. https://doi.org/10.5281/zenodo.13719678,

656   2024.

657 Wang, Y., Zheng, X., Dong, X., Xi, B., Wu, P., Logan, T., Yung, Y. L.: Impacts of long-range

658   transport of aerosols on marine-boundary-layer clouds in the eastern North Atlantic, Atmos.

659   Chem. Phys., 20(23), 14741-14755, https://doi.org/10.5194/acp-20-14741-2020, 2020.

660 Wehbe, Y., Tessendorf, S. A., Weeks, C., Bruintjes, R., Xue, L., Rasmussen, R., Lawson, P., Woods,

661   S., Temimi, M.: Analysis of aerosol-cloud interactions and their implications for

662   precipitation formation using aircraft observations over the United Arab Emirates, Atmos.

663   Chem. Phys., 21(16), 12543-12560, https://doi.org/10.5194/acp-21-12543-2021, 2021.

664 Wex, H., McFiggans, G., Henning, S., Stratmann, F.: Influence of the external mixing state of

665   atmospheric aerosol on derived CCN number concentrations, Geophys. Res. Lett., 37,

666   L10805, https://doi.org/10.1029/2010GL043337, 2010.

667 Wood,   R.:   Stratocumulus   clouds,   Mon.   Weather.   Rev.,   140(8),   2373-2423,

668   https://doi.org/10.1175/MWR-D-11-00121.1, 2012.

669 Yuan, T., Li, Z., Zhang, R., Fan, J.: Increase of cloud droplet size with aerosol optical depth: An

670   observation   and   modeling   study,   J.   Geophys.   Res-atmos.,   113,   D04201,

671   https://doi.org/10.1029/2007JD008632, 2008.

672 Zaveri, R. A., Wang, J., Fan, J., Zhang, Y., Shilling, J. E., Zelenyuk, A., Mei, F., Newsom, R., Pekour,

673   M., Tomlinson, J., Comstock, J. M., Shrinastava, M., Fortner, E., Machado, L. T., Artaxo,

674   P., Martin, S. T.: Rapid growth of anthropogenic organic nanoparticles greatly alters cloud

675   life   cycle   in   the   Amazon   rainforest,   Sci.   Adv.,   8(2),   eabj0329,

676   https://doi.org/10.1126/sciadv.abj0329, 2022.

677 Zelinka, M. D., Andrews, T., Forster, P. M., Taylor, K. E.: Quantifying components of aerosol-cloud-

678   radiation interactions in climate models, J. Geophys. Res-atmos., 119(12), 7599-7615,

679   https://doi.org/10.1002/2014JD021710, 2014.

680 Zhang, Q., Ma, X., Tie, X., Huang, M., Zhao, C.: Vertical distributions of aerosols under different

681   weather conditions: Analysis of in-situ aircraft measurements in Beijing, China, Atmos.

682   Environ., 43(34), 5526-5535, https://doi.org/10.1016/j.atmosenv.2009.05.037, 2009.

683 Zhang, Q., Quan, J., Tie, X., Huang, M., Ma, X.: Impact of aerosol particles on cloud formation:

684   Aircraft   measurements   in   China,   Atmos.   Environ.,   45(3),   665-672,

685   https://doi.org/10.1016/j.atmosenv.2010.10.025, 2011.

686 Zhao, C., Klein, S. A., Xie, S., Liu, X., Boyle, J. S., Zhang, Y. 2012. Aerosol first indirect effects on

687   non-precipitating low-level liquid cloud properties as simulated by CAM5 at ARM sites,

688   Geophys. Res. Lett., 39, L08806, https://doi.org/10.1029/2012GL051213, 2012.

689 Zhao, C., Qiu, Y., Dong, X., Wang, Z., Peng, Y., Li, B., Wu, Z., Wang, Y.: Negative aerosol-cloud

690   re relationship from aircraft observations over Hebei, China, Earth. Space. Sci., 5(1), 19-

691   29, https://doi.org/10.1002/2017EA000346, 2018.

692 Zhao, C., Zhao, L., Dong, X.: A case study of stratus cloud properties using in situ aircraft
693 observations over Huanghua, China, Atmosphere, 10(1), 19,
694 https://doi.org/10.3390/atmos10010019, 2019.

695 Zhao, Z. L., Mao, J. T., Wang, L.: In situ aircraft observations of one typical stratocumulus cloud
696 process compared with the satellite measurements, Acta. Meteorol. Sin., 69(03), 521-527,
697 http://dx.doi.org/10.11676/qxxb2011.045, 2011.